



Miniaturized implantable power transmission system for biomedical wireless applications

Shuoliang Ding, Stavros Koulouridis, Lionel Pichon

► To cite this version:

Shuoliang Ding, Stavros Koulouridis, Lionel Pichon. Miniaturized implantable power transmission system for biomedical wireless applications. Wireless Power Transfer, 2020, pp.1-9. 10.1017/wpt.2019.16 . hal-02502526

HAL Id: hal-02502526

<https://hal.science/hal-02502526>

Submitted on 11 Mar 2020

HAL is a multi-disciplinary open access archive for the deposit and dissemination of scientific research documents, whether they are published or not. The documents may come from teaching and research institutions in France or abroad, or from public or private research centers.

L'archive ouverte pluridisciplinaire **HAL**, est destinée au dépôt et à la diffusion de documents scientifiques de niveau recherche, publiés ou non, émanant des établissements d'enseignement et de recherche français ou étrangers, des laboratoires publics ou privés.

Miniaturized implantable power transmission system for biomedical wireless applications

Shuoliang Ding

Group of Electrical Engineering -Paris,
UMR 8507 CNRS,
CNRS, CentraleSupélec, Université
Paris-Sud, Sorbonne Université
Gif-sur-Yvette, France
shuoliang.ding@geeps.centralesupelec.fr

Stavros Koulouridis

Electrical and Computer Engineering
Department
University of Patras
Patras Greece
Koulouridis@upatras.gr

Lionel Pichon

Group of Electrical Engineering -Paris,
UMR 8507 CNRS,
CNRS, CentraleSupélec, Université
Paris-Sud, Sorbonne Université
Gif-sur-Yvette, France
lionel.pichon@geeps.centralesupelec.fr

Abstract— In this paper, a complete wireless power transmission scenario is presented, including an external transmission antenna, an in-body embedded antenna, a rectifying circuit and a powered sensor. This system operates at the Industrial, Scientific and Medical bands (ISM 902.8-928 MHz). For the antenna design, important parameters including reflection coefficient, radiation pattern and SAR are presented. As for the rectifying circuit, a precise model is created utilizing off-the-shelf components. Several circuit models and components are examined in order to obtain optimum results. Finally, this work is evaluated against various sensors' power needs found in literature.

Keywords— Implantable antenna, rectifying circuit, wireless power transmission, industrial, scientific and medical (ISM) band, Medical Device Radiocommunications (MedRadio) band.

I. INTRODUCTION

Implantable Medical Device (IMD) has gained scientist's attention nowadays. Thanks to recent development of the health care system, people now use more frequently IMDs in order to monitor continuously personal health conditions. IMDs should be light and small and able to serve various applications; they have thus huge potential. As one of the most used methods for wireless charging in large scale, microwave radiation has its own advantages: smaller and more robust to distance change and disorientations than other kinds of transmission methods, and perfectly meets the requirements for an IMD.

For biomedical uses, Medical Device Radiocommunication (MedRadio) Service band (401-406MHz) and the Industrial, Scientific and Medical (ISM) bands (433.1-434.8 MHz, 868-868.6 MHz, 902.8-928 MHz and 2.4-2.5 GHz) are authorized and frequently used [1-3]. A Radio Frequency (RF) medical energy transmission system consists of at least two parts: An antenna for capturing energy and a circuit for converting alternate current (AC) power to direct current (DC) power. The antenna supports energy transmission and sometimes data transmission as well. Among the bands that are mentioned above, the 902.8-928MHz band is frequently chosen as the energy transmission band.

As the most important part in the energy transmission system, the embedded antenna has been studied by many research teams in the world. Since the team of L.C. Chirwa [4] has published a study about the performances of an implanted source in human intestine under different frequencies in 2003, many research teams have carried out successively their own designs or analyses [5-7]. Some designs of antenna possess multiple resonant frequencies but have larger sizes [8]; others are smaller in size but resonate at higher frequency which will certainly lead to higher losses in deeper implantation [9]; moreover, many researches are performed in the skin layer, which adds difficulties to medical surgery and is less realistic [10-11].

There is also strong challenge for the design of the rectifying circuit. Since the input energy is extremely low, it is very difficult for the circuit to have a good efficiency due to all the losses in each component. Although many studies have been conducted on the rectifying circuit [12-13], circuits that operate with an input lower than -20dBm are not much studied. Still, there are published work that are focused on embedded rectifiers: H. W. Cheng et. al. has studied in [14] a rectenna system that operates at 400MHz with a circuit input power of 10dBm and rectifying efficiency of 76%. B. J. DeLong et. al. has proposed a rectenna structure that operates at 2.4GHz in free space, but the efficiency at -20dBm is only around 7% [15]. C. Liu et. al. has worked on an rectenna system which is implanted in body but only has an efficiency of 20% with an input power of -20dBm and implantation depth of 4mm [16]. In conclusion, due to its high operating frequencies and low input power level, the design of a deep-implanted and efficient energy transmitting rectenna is still a crucial challenge for researchers. Therefore, designing an adequate circuit that operates at low power input and matches with the antenna is also necessary.

In this paper, an integrated rectenna system is presented. Firstly, the receiving antenna design with all necessary parameters are presented. The presented antenna covers two frequency bands (MedRadio and ISM). MedRadio band will support the communication channel and is not discussed here. Then, a realistic rectifying circuit simulation is

studied. An electromagnetic electronic co-simulation is performed to evaluate and compare several designs in order to obtain the best results. Finally, some experimental results are presented while some current research work on sensors and their operation needs are detailed against present work. The target of this paper is to describe a complete embedded rectenna's working scenario.

II. EMBEDDED ANTENNA DESIGN

In this section, the design and key parameters of the embedded antenna are presented. All the calculations in this section is performed by CST Studio Suite 2017 [17].

A. Antenna design

A detailed parametric model of the designed antenna is presented in Fig.1. This antenna is made up of a circular radiating patch and a circular ground plane that are all printed on a circular substrate. Two circular slots are cut away from the patch so as to have two different operating frequencies at 402MHz and 915 MHz (MedRadio band and ISM bands). There is a shorting pin (radius = 0.15mm) located at point W in order to decrease the antenna size. The antenna is fed by a coaxial cable that is standardized to 50 Ω and located at point F. The entire antenna is covered by a superstrate. Both the substrate and the superstrate are of material Rogers RO3210 ($\epsilon_r=10.2$, $\tan\delta=0.003$) and have the same thickness of 0.64mm. All the necessary parameters are marked in Fig. 1 and detailed in Table. I.

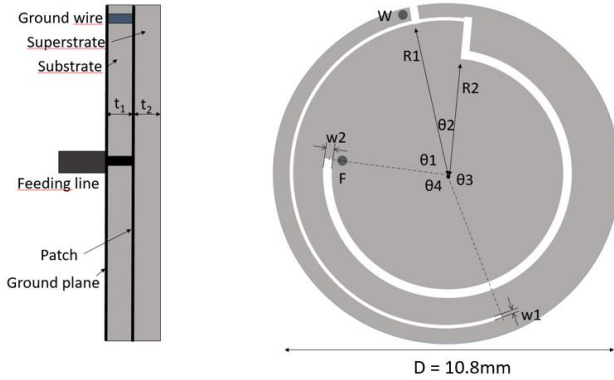


Fig.1. The circular antenna

TABLE I. ANTENNA PARAMETERS

Parameter Name	Value (mm)	Parameter Name	Value (deg)
R1	4.9	θ_1	70
R2	3.76	θ_2	18
w1	0.15	θ_3	163
w2	0.32	θ_4	109
t1	0.64		
t2	0.64		
D	10.8		

The whole antenna is embedded in a three-layer human arm model shown in Fig. 2. This model is made of three coaxial cylinder which simulate bone (radius: 0-25mm), muscle (radius: 25-47.5mm) where the antenna is embedded and skin (radius: 47.5-50mm). In order to save calculation

time, the length of the arm model is set to the minimum value that does not affect the results. The dielectric constants (relative permittivity ϵ_r and electrical conductivity σ) of the three types of human tissues at corresponding frequencies are presented in Table II.

The influence of the different positioning of the antenna is also investigated. Even if the maximum gain does not have significant difference between the two position, the positioning in xz plane allows more average gain at the front side, which is more favorable when the external antenna is not placed at the exact front of the implanted antenna.

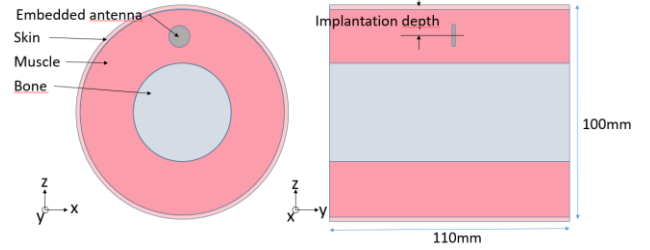


Fig.2. The three-layer arm model

TABLE II. DIELECTRIC CONSTANTS OF HUMAN TISSUE

Frequency		Bone	Muscle	Skin
403MHz	ϵ_r	13.22	57.15	46.81
	σ (S/m)	0.09	0.79	0.69
915MHz	ϵ_r	12.45	54.98	41.35
	σ (S/m)	0.15	0.93	0.85

B. Reflection coefficient

Reflection coefficient is a key factor to characterize an antenna. Fig.3 shows the reflection coefficient values at two different frequencies with different embedded depths varying from 10mm to 16mm.

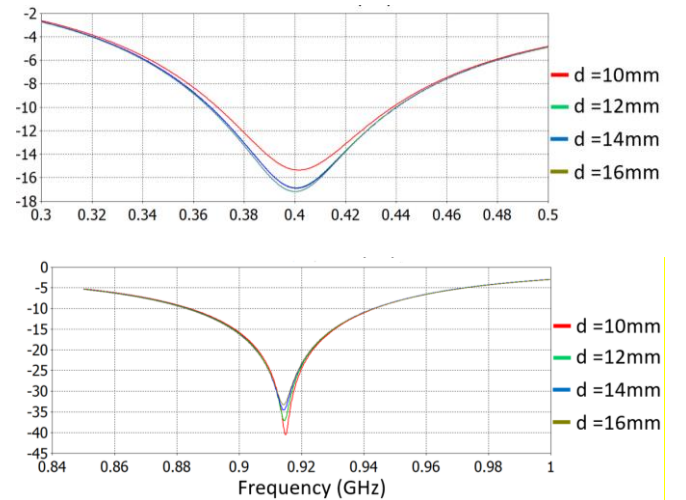


Fig.3. Reflection coefficient of the antenna (at 400MHz and at 915MHz)

As seen, the reflection coefficient values are almost immune to the change of implantation depth. The -10dB

bandwidths at 403MHz and 915MHz are 80MHz and 60MHz which cover the entire corresponding frequency band.

C. Radiation pattern, gain & SAR

The 2-D radiation patterns at the center of the operating frequency bands (403MHz and 915MHz) are presented in Fig. 4.

The antenna is embedded 10mm deep in arm. At MedRadio band (403MHz), the maximum gain in far field is around -33.5dB and towards Z axis. The value is low due to antenna's tiny size and deep implantation of 10mm in muscle. At ISM band (915MHz), the gain is -33.65dB. It is worth pointing out that the antenna has better maximum gain at deeper location: at 16mm depth, its gain increases to -31.6dB at 403MHz and -33.1dB at 915MHz since the radiation pattern has a narrower main lobe.

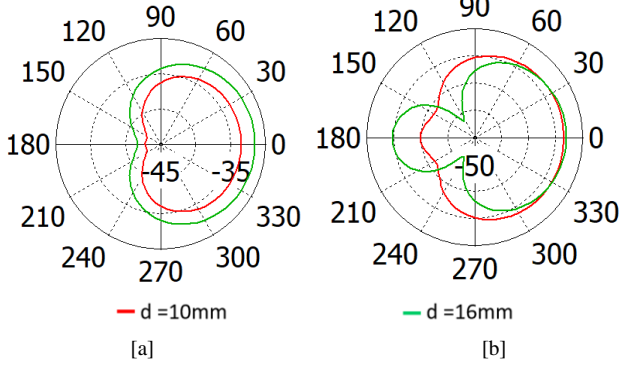


Fig.4. 2D radiation pattern of the antenna at 10 and 16mm implantation depth ([a] at 400MHz and [b] at 915MHz)

As an embedded antenna, safety issues are always of vital importance. Specific Absorption Rate (SAR) is the criterion for an IMD to evaluate its electromagnetic safety level. It indicates the average amount of power absorbed per unit of mass of human body. The two IEEE standards about SAR limits [18] [19] point out that the value of SAR of every 1g or 10g of human tissue cannot be higher than 1.6W/kg and 2W/kg respectively. In Table III, it is given the maximum input power for the embedded antenna that satisfies each SAR limits at 403MHz and 915MHz for implantation depths of 10 or 16mm.

TABLE III. MAXIMUM INPUT POWER FOR PIFA ANTENNA

Implantation depth (mm)	1g-average standard		10g-average standard	
	10mm	16mm	10mm	16mm
403MHz	15.38	14.99	72.22	71.17
	mW	mW	mW	mW
915MHz	14.08	14.01	86.33	91.19
	mW	mW	mW	mW

III. RECTIFYING CIRCUIT DESIGN

In this section, detailed parameters of the rectifying circuit and simulation results are presented.

A. Circuit Topology

The detailed design of the rectifying circuit is presented in Fig. 5

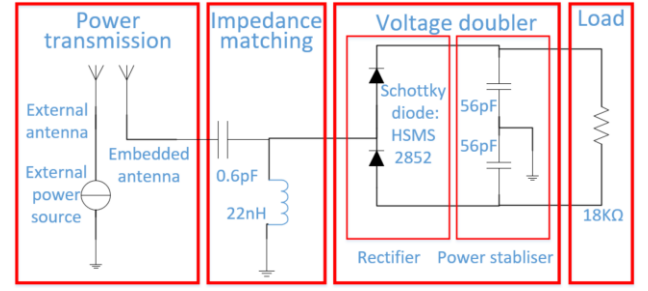


Fig.5. Rectenna system structure (abstract)

The entire rectenna system includes four sections in total. The first one is power transmission section proposed in the previous chapter. The external antenna transmits microwave power from outside the body into the embedded antenna, then the power flows through the voltage doubler in order to be converted into direct current (DC) power that could be used directly by the load. The impedance matching section ensures the minimization of power reflection.

The most important component in the rectifying circuit is the diode. As the circuit operates at 915MHz, ordinary diodes are not suitable. Two different diodes HSMS 285x series from Agilent Technologies and SMS 7630 series from Skyworks company were tested. The comparison results will be shown in part E in this chapter. HSMS 285x series are finally chosen.

B. Printed pattern design

In order to respect the size of the embedded antenna, the rectifying circuit must fit in a surface of the same size of the antenna. The proposed structure is presented in Fig. 6. Another circuit layer is added to back side of the antenna. The circuit is also printed on a substrate of the same thickness and material as the antenna, with the ground plane at the opposite side. Antenna's ground plane and circuit's ground plane are electrically connected and the circuit's feeding point is connected with the patch by a feeding line. The connection is a simple hole (radius = 0.15mm) that penetrate the substrate and the patch. Meanwhile, another hole (radius = 0.3mm) with the same center as the previous one is fabricated on the ground plane in order to avoid short-circuiting. Then the copper core of a coaxial cable goes through the hole and is soldered with the patch while the outside of the coaxial cable is soldered with the ground plane.

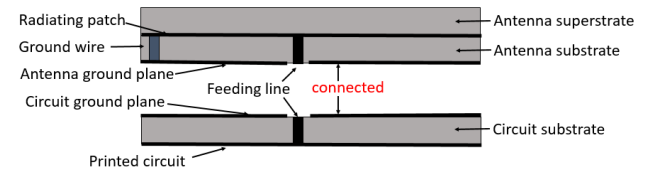


Fig.6. Rectenna system structure (physical)

In the circuit, the length and width of the circuit trace line generate impedance and phase changes in signal. The distance between the traces also causes parasitic phenomenon. Therefore, it is necessary to create an electromagnetic model for the circuit and run a co-simulation with lumped components so as to reach the best impedance matching results.

This co-simulation is performed by Advanced Design System 2019 [22] that supports at the same time electromagnetic modeling and circuit simulations. All the components that used in the simulation are off-the-shelf components from Murata company and are based on ADS's own library. The circuit pattern (copper circuit in red and substrate in green) is shown in Fig.7.

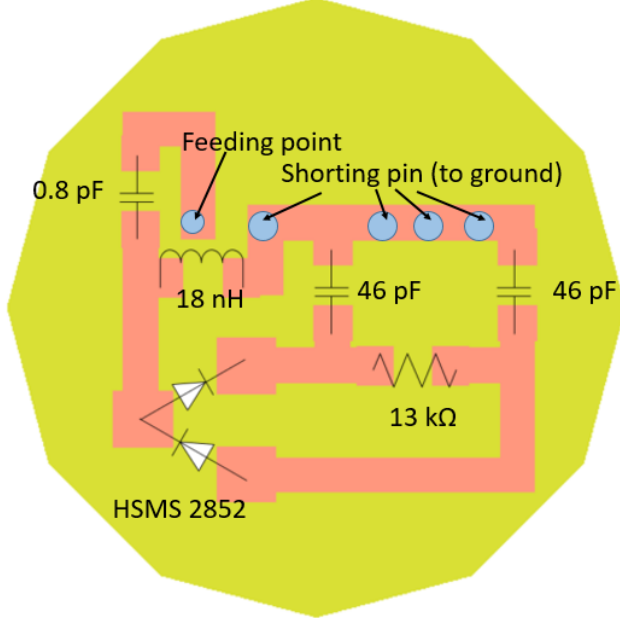


Fig.7. Rectifying system pattern

The values in Fig.7. are already adjusted to this circuit pattern and components' availability in order to achieve the maximum conversion efficiency.

C. Numerical results

In this section, numerical results that are based on ADS simulations are presented. Fig.8 shows the rectifying efficiency and output voltage (at load) for different input power level. The rectifying efficiency is the ratio between the power consumed by the load and the power provided by the power source. Because of reflection, the power provided by the source is slightly higher than the power consumed by the whole circuit.

Due to the existence of the non-linear component, there is a phase delay between the current and the voltage. Thus, input power is calculated by:

$$P_{active} = Re[U_{rms} * conj(I_{rms})] \quad (1)$$

where U_{rms} and I_{rms} are the voltage and the current in phasor form with the amplitude as root mean square (rms) values right after the receiving antenna respectively.

From the results shown in Fig. 8, it appears that when the source provides total power of -20dBm, the rectifying

efficiency is 31.15%, and the output voltage could achieve 0.195V. Comparing with the work in [23], the rectifying efficiency at -16dBm is 41.2% which is 10% better.

As the value of the load depends on different applications, it is also interesting to find the impact of load on the rectifying efficiency and output voltage. Fig. 9 shows different efficiency and output voltage as a function of different loads with -20 dBm power input.

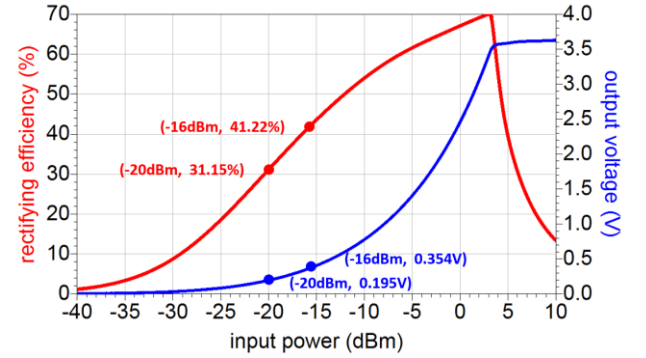


Fig.8. Efficiency and output voltage results for different input power (rectifying efficiency = 41.22%, output voltage = 0.354V with -16dBm input power; rectifying efficiency = 31.15%, output voltage = 0.195V with -20dBm input power)

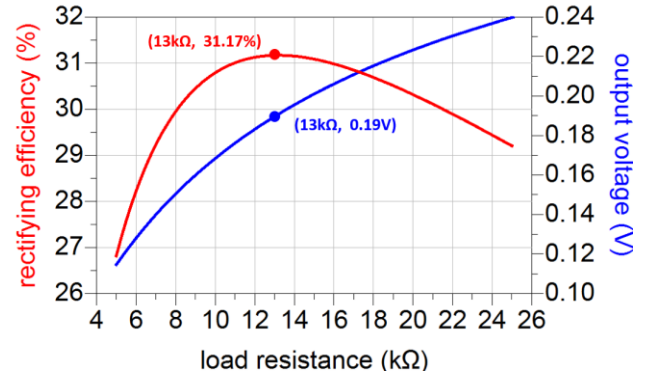


Fig.9. Efficiency and output voltage for different load resistance (rectifying efficiency = 31.17%, output voltage = 0.19V with 13kΩ load resistance)

As seen, the rectifying efficiency reaches a local peak value when load is 13KΩ. As the load increases, the power at the load decreases but the output voltage increases continuously, which might be used as voltage trigger.

D. Matching circuit comparison

There are many possibilities for the number of components in a matching circuit. In this section, a three-component matching circuit is presented in the aim of comparing with the two-component design and prove the superiority of the two-component design against other multiple component designs. The circuit is shown in Fig. 10.

In this design, the rectifying circuit consists of three different elements. Apart from this difference, the total lengths of transmission lines are even shorter than the previous design. However, the total efficiency is 23% at -

20dBm power input (shown in Fig. 11), which is less efficient than the previous two-component design.

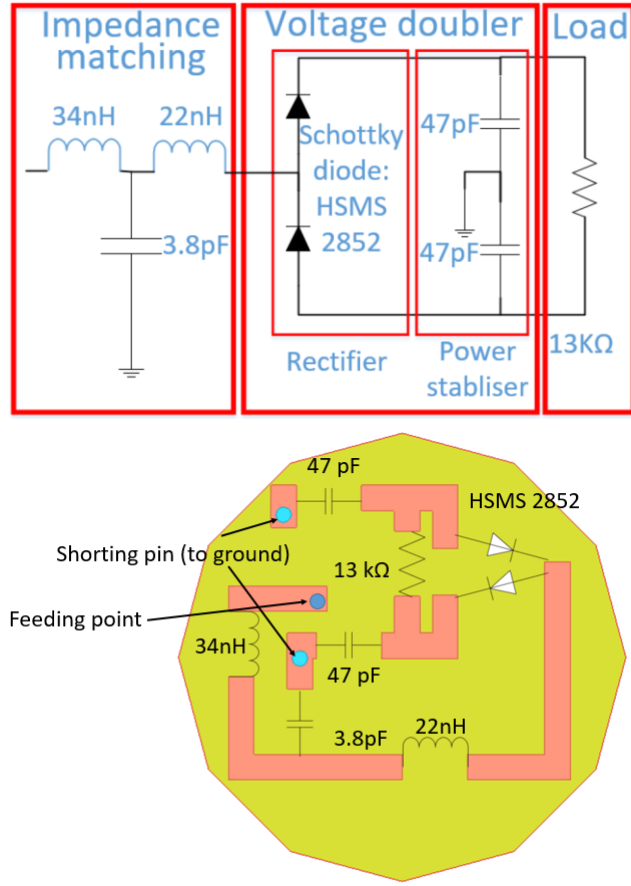


Fig.10. Three-component rectifying system design

E. Diodes comparison

Apart from matching circuits, the choice of diodes is also important. Skyworks 7630 and HSMS 2850 are both frequently used for low power rectifying. In this section, the performance of these two diodes are examined and compared in the same circuit pattern. The efficiency and output voltage are the main criteria for this comparison.

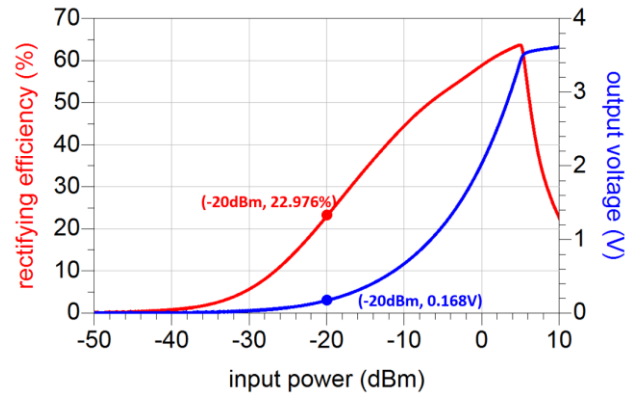


Fig.11. Efficiency and output voltage results for three-component design (rectifying efficiency = 22.976%, output voltage = 0.168V with -20dBm input power)

The ADS model of diode Skyworks 7630 is not provided by the Skyworks company. In this paper, a Spice model together with SOT-23 package model [24] is used as a realistic model for ADS simulation. Fig. 12 shows the rectifying efficiency and output voltage results for Skyworks 7630 diodes with different input power level.

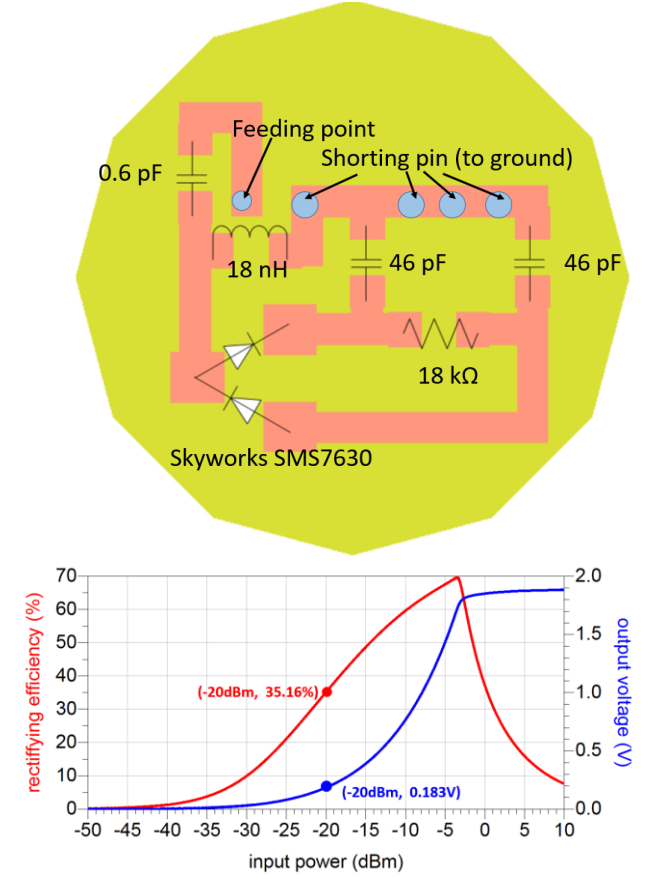


Fig.12. Topology and rectifying results for Skyworks 7630 diode (rectifying efficiency = 35.16%, output voltage = 0.183V with -20dBm input power)

Compared to the results in section C, the rectifying efficiency for this diode is 4% better than the previous model. However, this model is less accurate because it is created from the Spice parameters and SOT-23 package model. In contrast, HSMS 2850 exists already in the ADS library and is thus more trustworthy. In conclusion, although there is a tiny difference of rectifying efficiency between the two diodes, the HSMS 2850 diode is chosen for this rectifying circuit.

IV. EXPERIMENTAL RESULTS

A. Antenna test

During the experimental validation, minced pork is used for simulating human tissue and is put inside a plastic cup. The thickness of the cup is negligible. However, due to the fat component and air bubbles between the pork and cup, the dielectric constant of the simulated “human tissue” is smaller than normal muscle. Furthermore, it exists another layer of glue below the superstrate since it is glued

to the patch. Thus, some slight adjustments should be done to the antenna design before the fabrication.

The embedded antenna is fabricated, soldered together with the coaxial cable, then stick with superstrate by glue. A network analyzer is used to measure the reflection coefficient of the antenna. The fabricated antenna is shown in Fig. 13.

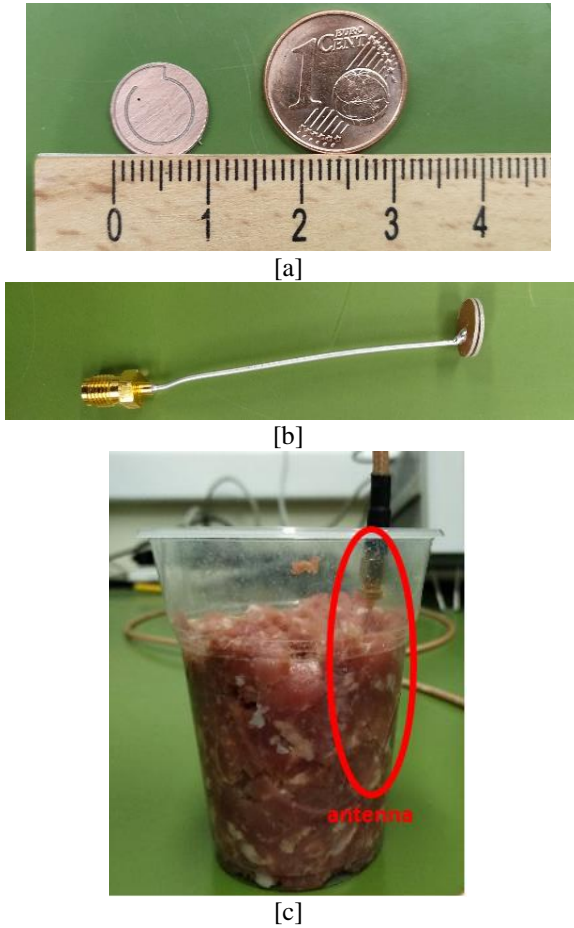


Fig.13. [a] fabricated antenna comparing with one euro cent
[b] complete antenna with coaxial cable and superstrate
[c] antenna embedded into minced pork

Unlike the ideal simulation environment, the real case is more complicated and more difficult to control.

In the simulation, the metallic radiating patch has the same size as the substrate, which leads to a direct contact with the minced pork meat. Due to this contact, the resistance (the real part of the impedance) of the antenna at its first resonant frequency (403MHz) is smaller and the reactance (the imaginary part of the impedance) of the second resonant frequency (915MHz) is larger than without contact.

However, in the real case, some glue is used so as to stick the superstrate with the substrate. For the first measurement, since the edge of the metallic patch is thin, some glue covered it and hence isolate it from the surrounding minced pork meat, which avoided the contact mentioned before and thus made the resistance at 403MHz higher and the reactance at 915MHz lower. Therefore, the

reflection coefficient at 403MHz is around -6dB instead of -20dB (in simulation) and the second resonant frequency is at 1.04GHz instead of 915MHz (in simulation). The corresponding measurement results are shown in Fig. 14[a]. Because the results are different from those of the previous simulations, another simulation in which the metallic patch is surrounding by 0.3mm of glue was done, the results are also shown in the same figure, which matches well the measurement result. This simulation model is presented in Fig.14[b].

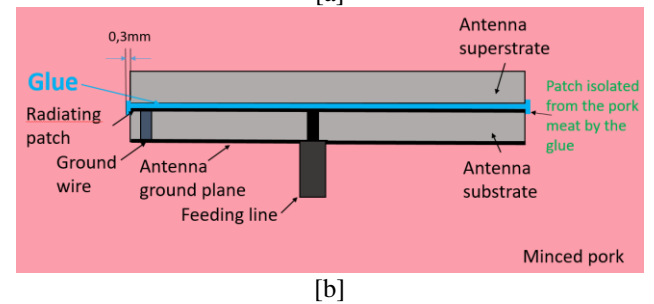
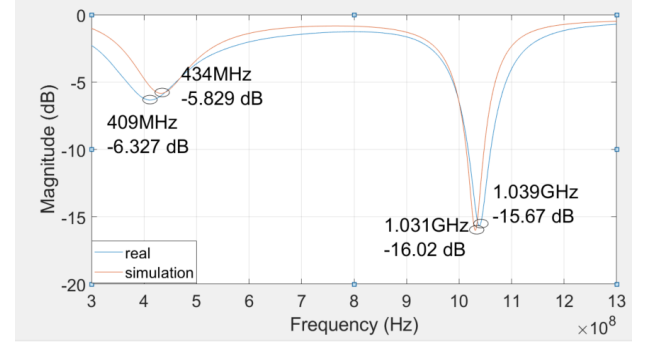


Fig.14. [a] First measurement results and corresponding simulation when patch is isolated by glue [b] corresponding simulation model

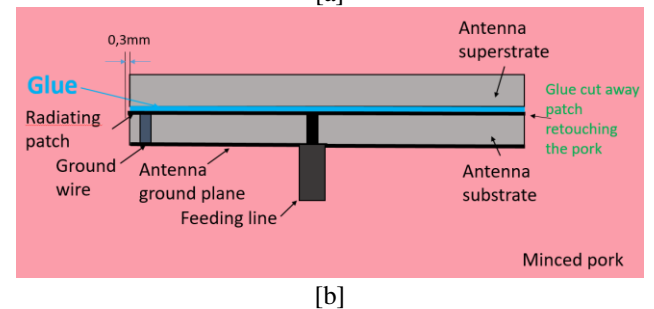
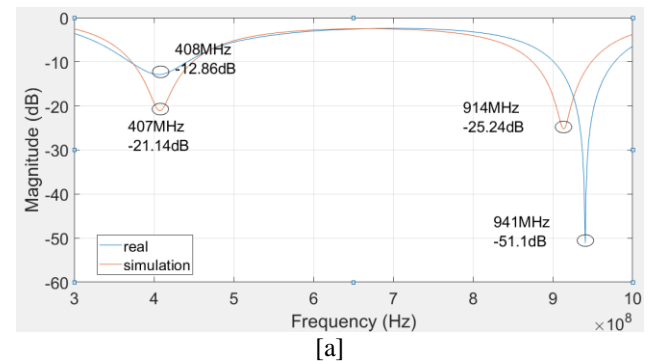


Fig.15. [a] Second measurement results and corresponding simulation when patch is expose to the minced pork meat [b] corresponding experimental model

Meanwhile, in order to confirm the results from the design in previous chapters, a second measurement is done with the surrounding glue cut away from the antenna (patch exposed to pork meat). Fig. 15[a] shows the comparison of the measurement and simulation results. There is still slight difference which is probably caused by air bubbles in the minced pork. The experimental results matches globally the simulation results.

B. Circuit test

As an essential part of the power transmission system, the circuit is tested separately in order to measure its performance. Fig. 16 shows the unsoldered and soldered circuit. The circuit is fed by a coaxial cable from Pasternack company.

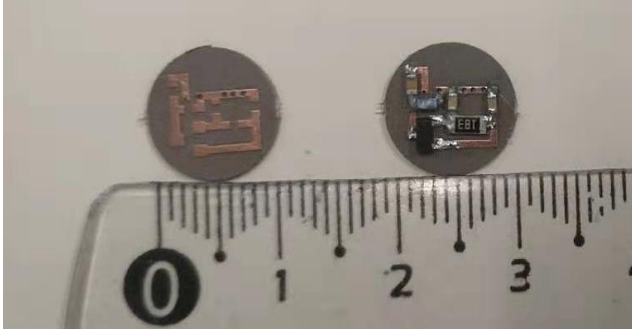


Fig.16. Soldered and unsoldered circuits

The measurement is performed by the RHODES & SCHWARZ ZNB Vector Network Analyzer (VNA). The VNA provide -20dBm of power from its output port for the circuit. The impedance of the total circuit and the voltage between the load are measured during the experiment. The load is a 18k Ω resistance instead of a 13k Ω but the results difference is negligible.

The total impedance of the circuit is around 32-31j Ω , which is nearly matched with the standard 50 Ω impedance at 915MHz. The reflection coefficient is -7.8 dB. The voltage at the load is measured as 0.07V by a multimeter placed at the two ends of the 18k Ω load. The value presents some difference with the simulation results, which is likely due to the tiny size of the circuit. The measurement impedance could even be affected by the different size of soldering dot. Some more advanced experiments are still undergoing.

V. SENSORS POWERING

Various micro-sensor grids for biomedical uses are studied and developed in recent years. These sensors cost low power and have small sizes to be suitable for implanting uses. In Table. IV, several sensors together with its feeding power, supply voltage, area of circuit and Effective Number of Bits (ENOB) are presented.

As seen, the sensors in the table require low energy and voltage to operate. They also occupy little space which is suitable for implanted uses together with the power transmission system in this paper. In order to match the two parts together, it is necessary to calculate the actual power that received by the load.

TABLE IV. LOW COST SENSORS AND SPECIFIC PARAMETERS

Ref	Average power consumption (μ W)	Supply Voltage (V)	Area (mm^2)	ENOB (bit)
[25]	5.5	0.5	375	8.02
[26]	0.27	0.3	0.07	6.1
[27]	6.9	3	9.28	8
[28]	10.5	1.8	0.25	13
[29]	1.5	1	2.25	12

From the previous calculation, the power that a single power transmission system in this paper could receive for different transmission distances is shown in Table. V.

TABLE V. RECEIVED POWER AT DIFFERENCE DISTANCES

Transmission distance (mm)	Rectifying efficiency (%)	Voltage at load (V)	Power at load (μ W)
200	44.5	0.412	31.98
240	39.0	0.294	18.58
280	34.5	0.225	12.13
320	31.4	0.184	9.11
360	27.8	0.145	6.52
400	23.2	0.108	4.33

As shown in Table. V, the power transmission system is capable of feeding several sensors in terms of power. The mentioned results are calculated by simulations. These results are calculated by the power that received by the implanted antenna with the corresponding distance value and the rectifying efficiency & output voltage results with the corresponding power received. In both simulations, the port impedances are standardized to 50 Ω .

For the values in table V, the power at the input of the rectifying circuit is not always -20 dBm. This power varies with the change of transmission distances. However, due to the reference [21], the power emitted by the external antenna must not be higher than 30dBm. Therefore, in all the results presented in table V, the power emitted by the external antenna is fixed at the maximum value 30dBm. When the external antenna is located 200mm away from the human body, the implanted antenna can receive around 32 μ W at load. This could support anyone of the sensors that mentioned in Table. IV. However, a voltage booster is still needed for achieve the supply voltage of the sensors and will be tested in the future.

CONCLUSION

A miniature wireless power transmission system for biomedical uses is presented in this paper. A complete scenario from external antenna to sensor powering is detailed and discussed. This power transmission system operates at 915MHz. Several simulations are done for both the antenna and the rectifying circuit part. A comparison of the numerical predictions with experimental measurements proved the validity of the global system. The dual-band embedded antenna could receive around 77 μ W from an external patch antenna at 200mm in distance and then 44.5% of it could be converted into DC power, which is around 32 μ W in total. At 400mm distance, the received DC power decreases to 4.33 μ W. In addition, it is also tested that the

circuit is capable of rectifying AC into DC power with an optimum efficiency. Some experimental results are obtained and more accurate results are under procedure. In the last section, it is proved that this system could support the feeding of several kinds of sensors in terms of received power.

For the future work, several single systems could be combined together and operate at the same time in order to increase the output voltage and rectifying power. An external signal enhancing solution could also be possible.

REFERENCES

- [1] "International Telecommunications Union-Radiocommunications (ITU-R), radio regulations, section 5.138 and 5.150," ITU. Geneva, Switzerland, [Online].
- [2] S. Bakogianni, and S. Koulouridis, "An implantable planar dipole antenna for wireless medradio-band biotelemetry devices," *IEEE Antennas Wireless Propag. Lett.*, vol. 15, pp. 234-237, 2016.
- [3] FCC. Washington, D.C., USA, Federal Communications Commission 2012. [Online]. Available online: <http://www.fcc.gov>
- [4] Chirwa, L. C., Hammond, P. A., Roy, S., & Cumming, D. R. S. (2003). Electromagnetic radiation from ingested sources in the human intestine between 150 MHz and 1.2 GHz. *IEEE Transactions on Biomedical Engineering*, 50(4), 484-492.
- [5] Kim, J., & Rahmat-Samii, Y. (2004). Implanted antennas inside a human body: Simulations, designs, and characterizations. *IEEE Transactions on Microwave Theory and Techniques*, 52(8 II), 1934-1943.
- [6] Luu, Q. T., Koulouridis, S., Diet, A., Le Bihan, Y., & Pichon, L. (2017). Investigation of inductive and radiating energy harvesting for an implanted biotelemetry antenna. *2017 11th European Conference on Antennas and Propagation, EUCAP 2017*, 160-163.
- [7] Ali, M. M., Bashar, M. E. I., & Hosain, M. K. (2017). Circular Planner Inverted-F Antenna for Implantable Biomedical Applications. *2017 2nd International Conference on Electrical & Electronic Engineering (ICEEE)*, 1, 1-4.
- [8] Liu, C., Guo, Y. X., & Xiao, S. (2012). Compact dual-band antenna for implantable devices. *IEEE Antennas and Wireless Propagation Letters*, 11, 1508-1511.
- [9] Kiourti, A., & Nikita, K. S. (2012). Miniature scalp-implantable antennas for telemetry in the MICS and ISM bands: Design, safety considerations and link budget analysis. *IEEE Transactions on Antennas and Propagation*, 60(8), 3568-3575.
- [10] Karacolak T., Cooper R., & Topsakal, E. (2009). Electrical properties of rat skin and design of implantable antennas for medical wireless telemetry. *IEEE Transactions on Antennas and Propagation*, 57(9), 2806-2812.
- [11] Mohamed, A. E., & Sharawi, M. S. (2017). Miniaturized dual-wideband circular patch antenna for biomedical telemetry. *2017 11th European Conference on Antennas and Propagation (EUCAP)*, 1027-1030.
- [12] H. Visser, S. Keyrouz & A. Smolders (2015). Optimized rectenna design, *Wireless Power Transfer* (2015). 2(1), 44-50. Cambridge University Press.
- [13] Asif, S. M., Ifthikhar, A., Hansen, J. W., Khan, M. S., Ewert, D. L., Braaten, B. D., & Member, S. (2019). A Novel RF-Powered Wireless Pacing via a Rectenna-Based Pacemaker and a Wearable Transmit-Antenna Array. *IEEE Access*, 7, 1139-1148.
- [14] H. Cheng, T. Yu and C. Luo, "Direct current driving impedance matching method for rectenna using medical implant communication service band for wireless battery charging," in *IET Microwaves, Antennas & Propagation*, vol. 7, no. 4, pp. 277-282, 19 March 2013.
- [15] B. J. DeLong, A. Kiourti and J. L. Volakis, "A Radiating Near-Field Patch Rectenna for Wireless Power Transfer to Medical Implants at 2.4 GHz," in *IEEE Journal of Electromagnetics, RF and Microwaves in Medicine and Biology*, vol. 2, no. 1, pp. 64-69, March 2018.
- [16] C. Liu, Y. Guo, H. Sun and S. Xiao, "Design and Safety Considerations of an Implantable Rectenna for Far-Field Wireless Power Transfer," in *IEEE Transactions on Antennas and Propagation*, vol. 62, no. 11, pp. 5798-5806, Nov. 2014.
- [17] Computer Simulation Technology (CST) STUDIO SUITE. Ver 2017, CST AG, Germany
- [18] IEEE standard for safety levels with respect to human exposure to radiofrequency electromagnetic fields, 3 kHz to 300 GHz, IEEE Standard C95.1, 1999.
- [19] IEEE standard for safety levels with respect to human exposure to radiofrequency electromagnetic fields, 3 kHz to 300 GHz, IEEE Standard C95.1, 2005
- [20] International Telecommunications Union. (1998). Recommendation ITU-R RS.1346.
- [21] FCC 15. 209, Standard Specification for Radiated emission limits, general requirements
- [22] Advanced Design System (ADS) 2019, Keysight Technology.
- [23] S. Bakogianni and S. Koulouridis, "Design of a novel miniature implantable rectenna for in-body medical devices power support," *2016 10th European Conference on Antennas and Propagation (EuCAP)*, Davos, 2016, pp. 1-5.
- [24] APN1001: Circuit Models for Plastic Packaged Microwave Diodes, Skyworks application note
- [25] Trung, N. T., Häfliger, P., & Member, S. (2015). A Submicrowatt Implantable Capacitive Sensor System for Biomedical Applications. *IEEE Transactions on Circuits and Systems II: Express Briefs*, 62(2), 209-213.
- [26] H. Danneels, K. Coddens and G. Gielen, "A fully-digital, 0.3V, 270 nW capacitive sensor interface without external references," *2011 Proceedings of the ESSCIRC (ESSCIRC)*, Helsinki, 2011, pp. 287-290.
- [27] Bracke, W., Merken, P., Puers, R., Member, S., & Hoof, C. Van. (2007). Ultra-Low-Power Interface Chip for Autonomous Capacitive Sensor Systems, *54(1)*, 130-140.
- [28] Z. Tan *et al.*, "A 1.8V 11 μ W CMOS smart humidity sensor for RFID sensing applications," *IEEE Asian Solid-State Circuits Conference 2011*, Jeju, 2011, pp. 105-108.
- [29] M. Kamarainen *et al.*, "A 1.5 μ W 1V 2nd-Order $\Delta\Sigma$ Sensor Front-End with Signal Boosting and Offset Compensation for a Capacitive 3-Axis Micro-Accelerometer," 2008 IEEE International Solid-State Circuits Conference - Digest of Technical Papers, San Francisco, CA, 2008, pp. 578-637.